

Catalysis Science & Technology

Accepted Manuscript

This article can be cited before page numbers have been issued, to do this please use: G. Zhao, W. guandong, Y. Liu, Y. He, J. Feng and D. Li, *Catal. Sci. Technol.*, 2020, DOI: 10.1039/D0CY00356E.



This is an Accepted Manuscript, which has been through the Royal Society of Chemistry peer review process and has been accepted for publication.

Accepted Manuscripts are published online shortly after acceptance, before technical editing, formatting and proof reading. Using this free service, authors can make their results available to the community, in citable form, before we publish the edited article. We will replace this Accepted Manuscript with the edited and formatted Advance Article as soon as it is available.

You can find more information about Accepted Manuscripts in the [Information for Authors](#).

Please note that technical editing may introduce minor changes to the text and/or graphics, which may alter content. The journal's standard [Terms & Conditions](#) and the [Ethical guidelines](#) still apply. In no event shall the Royal Society of Chemistry be held responsible for any errors or omissions in this Accepted Manuscript or any consequences arising from the use of any information it contains.

The preparation of AuPd/ZnO-CuO for directional oxidation of glycerol to DHA.

Gengqiang Zhao^{a,b,1}, Guandong Wu^{a,b,1}, Yanan Liu^{a,b}, Yufei He^{a,b*}, Junting Feng^{a,b}, Dianqing Li^{a,b*}

^aState Key Laboratory of Chemical Engineering, Beijing University of Chemical Technology, Beijing 100029, China

^bBeijing Engineering Center for Hierarchical Catalysts, Beijing University of Chemical Technology, Beijing 100029, China

¹Gengqiang Zhao and Guandong Wu contributed equally to this work.

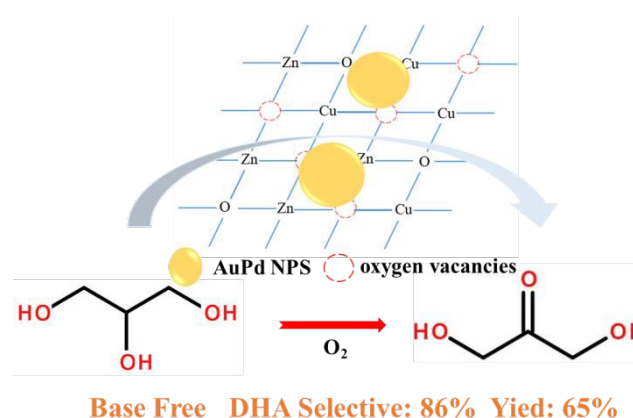
*Corresponding authors at: State Key Laboratory of Chemical Engineering, Beijing University of Chemical Technology, Beijing 100029, China.

E-mail address: yfhe@mail.buct.edu.cn (Y. F. He).

ABSTRACT

View Article Online
DOI: 10.1039/D0CY00356E

Selective activation of the C-O bond of glycerol is a considerable challenge in current academic research. Herein, we fabricate an efficient AuPd/ZnO-CuO catalyst by a simple precipitation method and use it in the selective oxidation of glycerol (GLY) to produce



dihydroxyacetone (DHA). Under the base free condition, AuPd/ZnO-CuO catalyst exhibits the preferable catalytic performance compared with AuPd/ZnO and AuPd/CuO. The turnover frequency (TOF) of AuPd/ZnO-CuO reaches 687.1 h^{-1} , which is 25 times that of AuPd/CuO and 6 times that of AuPd/ZnO. AuPd/ZnO-CuO catalyst also shows good selectivity towards DHA and the highest DHA yield is 65.3 %, which is at the top level among the reported results. Through the STEM-EDS, XRD and Raman analysis, we find that ZnO-CuO is a composite oxide and Zn and Cu elements in the ZnO-CuO support are uniformly distributed. Furthermore, HRTEM, EPR and XPS results show that AuPd/ZnO-CuO has smaller AuPd alloy nanoparticles (NPs) but higher concentration of surface defect sites compared with AuPd/ZnO and AuPd/CuO. Together with the catalytic performance and feasible mechanism, we consider that the enhanced performance of AuPd/ZnO-CuO catalyst could be mainly ascribed to the rich surface defect sites, which facilitate the adsorption and activation for the secondary hydroxyl groups of glycerol.

1. Introduction

Selective activation of carbon-oxygen bonds is a huge challenge of current academic research and industrial application. GLY, a major by-product produced during the production of biodiesel, has received intense attention due to its highly functional group. Selective oxidation of glycerol is an effective method for producing high value-added chemicals [1-3]. However, the selective oxidation of glycerol is extremely difficult and complex, involving the issues of selective activation of C-O bond (primary hydroxyl group or secondary hydroxyl group), the degree of oxidation as well as the C-C bond cleavage [4,5]. Therefore, much attention should be paid to fabricate a catalyst to achieve the goal of high selectivity in the oxidation of glycerol reaction.

In all the glycerol oxidation product, Dihydroxyacetone (DHA) produced by the oxidation of glycerol secondary alcohol group can be widely used in medicine, biology, cosmetics and other organic synthesis industry. Researchers around the world have been working hard to prepare suitable catalysts for this process [6-8]. Bimetallic catalysts based on Pt or Pd showed promising catalytic performance, but the oxidation reaction mainly happened over primary hydroxyl groups [9-13]. In the selective oxidation of secondary hydroxyl groups of glycerol, Au exhibited higher selectivity than Pt or Pd catalysts [14-19]. For example, Xu and his partners prepared a sequence of Au/MO_x catalysts and proved that they were viable catalysts for the oxidation of glycerol to DHA [20]. Moreover, the catalytic performance was directly related to the amount of the oxygen vacancies and the state of the Au species. In our previous research, it was found that oxygen vacancies in Au/ZnO interface could specifically adsorb glycerol secondary hydroxyl groups and then selectively oxidize glycerol to DHA [21,22]. Even progress in the oxidation of secondary glycerol alcohol has been made. Further study is still imperative to enhance the efficiency in this process to meet the needs of industrialization.

In the oxidation of alcohol, alloying is generally considered to modify the Au based active sites to improve the activation of oxygen. For example, AuPd NPs prepared by colloidal methods exhibited better performance than the corresponding single metal catalysts in the liquid phase oxidation of glycerol with the addition of base [23]. Moreover, the nature of the support also affected catalytic performance [24]. For AuPd catalysts, when a basic oxide was used as the support, the catalyst had enhanced activity in the oxidation of glycerol. However, the C-C bond was severely broken and the selectivity of the target C₃ product was limited. When an acidic oxide was employed, the chain scission was significantly reduced, but the activation of glycerol was seriously insufficient [25,26]. It is reported that the number of oxygen vacancies was closely connected to the support component. Wang et al. showed that doping Cu into CeO could cause more defects on the surface of CeO, which provided more reaction sites for the adsorption and activation of CO₂ to improve the efficiency of methane production [27]. The above results show that the nature of the support plays an important role in the selective oxidation of glycerol, and subtle control of the catalyst should be taken to increase the activity without destroying the selective oxidation towards the secondary hydroxyl.

Herein, we prepare a ZnO-CuO composite oxide support by a single drop method and an AuPd/ZnO-CuO catalyst is then synthesized by the precipitation method. For comparison, the corresponding single metal catalysts supported on ZnO-CuO and AuPd bimetallic catalysts on ZnO or CuO are also prepared. The obtained catalysts are used in the selective oxidation of glycerol and an obvious enhancement in the activity over AuPd/ZnO-CuO catalyst is observed. Based on the STEM-HAADF, Raman, EPR and catalytic test results, the effect of the active component alloying and the nature of support on catalytic performance is discussed.

2. Experimental Section.

2.1. Materials.

Zn(NO₃)₂·6H₂O, NaOH, Cu(NO₃)₂·3H₂O, urea, HAuCl₄·3H₂O, Na₂PdCl₄, glycolic

acid (GCA), and DHA were A.R. grade, while glycerol and acetonitrile were HPLC grade. Deionized water was made in the laboratory and its conductivity was below 10^{-6} S/cm.

2.2. Preparation of ZnO-CuO supports.

6.04 g of $\text{Cu}(\text{NO}_3)_2 \cdot 3\text{H}_2\text{O}$ and 7.44 g of $\text{Zn}(\text{NO}_3)_2 \cdot 6\text{H}_2\text{O}$ were added to 150 ml of deionized water and sonicated to obtain a light blue transparent solution. Then, 100 ml of NaOH solution (1 mol/L) was added dropwise to the transparent solution at a rate of 100 ml/h, followed by vigorous stirring for 2 h at 25 °C. The reaction solution was centrifuged and the precipitate was washed with deionized water five times. After drying at 75 °C for 12 h, the solids were ground to 40-70 mesh. The powder was calcined in air at 600 °C for another 6 h with a heating rate of 5 °C/min to obtain ZnO-CuO oxide support. CuO and ZnO oxides are also prepared by the same method.

2.3 Preparation of AuPd catalysts.

The AuPd/ZnO-CuO catalyst was prepared by the deposition-precipitation (DP) method. ZnO-CuO support (0.60 g) was added to the solution containing Na_2PdCl_4 and HAuCl_4 necessary to obtain the theoretical loading of 2 wt.% Au (Au: Pd = 10:1). Then a certain mass of urea (urea/Au = 500:1 mol/mol) was added to the solution. After the mixed solution was sonicated for 5 min, it was transferred to a 90 °C water bath and stirred for 4 h. The reaction solution was centrifuged and the precipitate was washed with deionized water three times. We grind the solids to 40-70 mesh after being dried at 80 °C for 10 h in an oven. The powder was calcined in air at 300 °C for 3 h with the heating rate of 2 °C/min to obtain the AuPd/ZnO-CuO catalyst. AuPd/CuO, AuPd/ZnO catalysts and single metal catalysts are also prepared by the same method.

2.4 Characterization

The crystal structures of ZnO-CuO was identified by XRD (Shimadzu XRD-600). Cu $K\alpha$ radiation source wavelength was 0.154 nm. The sample morphology was observed by scanning electron microscopy (Zeiss Supra 55). The BET data of the samples were tested with the Gemini VII 2390 instrument. The element content and

distribution was tested by STEM-EDS (JEOL-2100F) and ICP-AES (Shimadzu ICP-7500). Fourier transform infrared (FTIR) spectra were recorded by Bruker Vector 22 spectrometer. Raman spectroscopy (Renishaw, inVia-Reflex, 633 nm) was used to obtain Raman signals for the three samples. Active component state and particle size of three catalysts were characterized by high angle annular dark field image (STEM-HAADF, JEOL-2100F). X-ray photoelectron spectroscopy (XPS) spectra were obtained using a Thermo VG ESCALAB 250 spectrometer with a C 1s peak at 284.6 eV and Al K α as the anode. Electron paramagnetic resonance (EPR) spectra were obtained using a Bruker EMX-500 10/12 spectrometer at 100K. FTIR of glycerol was collected using subtraction spectrum mode. First, 0.50 g of the catalysts were placed in 5 ml of 0.1 M glycerol and stirred for 0.5 h. After centrifugation, the catalysts were placed in freeze-drying to remove excess water. The spectra of the catalysts and the pure catalysts were collected in a high vacuum. The spectra of the catalysts and the pure catalysts are subtracted to obtain the infrared spectrum of glycerol adsorbed on the catalysts.

2.5. Glycerol Oxidation Test

10 ml of GLY (0.05 M) and catalyst (glycerol/Au=100 molar ratio) were added to a 50 ml quartz bottle and the air in the reaction system was replaced with oxygen for 2 min. Then we placed it on a parallel reactor to start the reaction (reaction conditions: temperature 80 °C, speed 900 r/min, pressure 0.1 MPa). After the reaction was completed, the reactor was quickly put into the cold water bath and cool to room temperature. The reaction solution was filtered with the disposable organic filter (0.22 μ m) to obtain transparent liquid. We used HPLC to quantify the type and content of substances in our reaction solution. Our mobile phase is H₃PO₄ (0.1 wt.%, 0.2 mL/min) and acetonitrile (0.4 mL/min). The column type is Zorbax SAX column and the test temperature is 30 °C. Ultraviolet detector (210 nm) and refractive index detector are our detectors. The contents of glycerol and liquid products were measured by the external calibration method. The Glycerol (GLY) conversion, product selectivity, DHA

yield, and TOF for different catalysts were calculated as follows:

$$\text{GLY conversion (\%)} = M_{\text{converted GLY}}/M_{\text{GLY in feed}} \times 100,$$

$$\text{Product selectivity (\%)} = M_{\text{product}}/M_{\text{converted GLY}} \times 100,$$

$$\text{DHA yield \%} = \text{GLY conversion (\%)} \times \text{DHA selectivity (\%)} / 100,$$

$$\text{TOF} = M_{\text{converted GLY}} / [M_{\text{surface Au atoms}} \times \text{time(h)}],$$

Surface Au atom number is calculated by particle size formula,

Surface Au atoms = $0.90d^{0.7}$, where d is the Au particle size measured by HRTEM [28,29].

The TOF of the catalysts were calculated under 15 % glycerol conversion.

3. Results and discussion

3.1 Catalytic Performance

Aerobic oxidation of glycerol was carried out using the AuPd/CuO, AuPd/ZnO, AuPd/CuO-ZnO catalysts. As shown in **Figure 1(A)**, glycerol conversion increases with time, and AuPd/CuO-ZnO catalyst always exhibits higher glycerol conversion. Specifically, the conversion of glycerol on the AuPd/CuO-ZnO catalyst is 92.7 % at 4 h, while the conversion on AuPd/CuO and AuPd/ZnO catalyst is only 16.0 % and 48.0 %. In our research system, DHA is the target product. In **Figure 1(B)**, when the reaction time reaches 2 hours, the maximum yield (65.3 %) of DHA over the AuPd/ZnO-CuO catalyst is achieved. The maximum DHA yield over AuPd/CuO and AuPd/ZnO is observed at 4h, and the value is only 12.6 % and 35.8 %. The above results show that AuPd/ZnO-CuO catalysts are more capable of oxidizing glycerol to DHA.

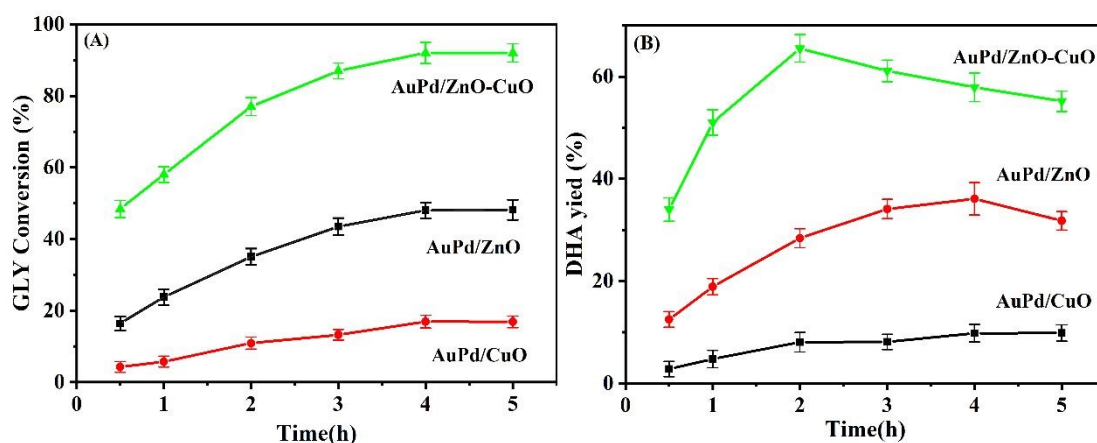


Figure 1. Glycerol conversion versus time curve (A), and DHA yield versus time curve (B). Reaction conditions: glycerol/Au = 100 mol/mol, 80 °C, 1 bar O₂, 900 rpm stirrer speed.

The TOF value of AuPd/CuO, AuPd/ZnO, AuPd/ZnO-CuO catalysts are calculated and listed in **Table 1**. The TOF value of the AuPd/ZnO-CuO catalyst is 25 times and 6 times than that of AuPd/CuO and AuPd/ZnO. For comparison, we prepare monometallic Pd and Au catalyst on ZnO-CuO support. It can be seen that the DHA yield and TOF value of the bimetallic catalyst are significantly higher than those of the single metal catalyst. Furthermore, we change the ratio of Zn: Cu in AuPd/ZnO-CuO catalysts and find that the catalyst with 1:1 of Zn: Cu shows the highest catalytic performance. It is also noted that the carbon balance over AuPd/ZnO-CuO catalysts is always more than 97 %. In the selective oxidation of glycerol towards DHA, Pt-based catalysts also showed good performance and some excellent performance data are listed in **Table 1** [30,31]. Compared with the reported Pt-based catalyst, a noticeable increase in both TOF and DHA yield over AuPd/ZnO-CuO is seen. We also examine the oxidation product distribution for different catalysts. The by-products over the Pt-based catalyst is mainly glyceric acid (GLYA) and glyceraldehyde (GLD), which are oxidized from the primary hydroxyl of glycerol. However, in the case of AuPd/ZnO-CuO, we detect CO₂ and glycolic acid as the main by-products and no glyceric acid as a by-product that is often found in the literature. Specifically, at 75 % glycerol conversion, the selectivity of DHA over AuPd/ZnO-CuO is 86 %, and gas-phase products account for about 7.3 %. The DHA selectivity of Pt-based catalysts is less than 55 %, and the by-products are mainly glyceraldehyde and glyceric acid, which account for about 30 %. The different product distribution indicates that the oxidation pathway of glycerol is different between Au-based catalyst and Pt-based catalyst and AuPd/ZnO-CuO catalyst can be directed to activate the secondary hydroxyl group. Moreover, we obtain time-conversion curves at different temperatures and calculate the apparent activation energy (E_a) of the three catalysts, according to the Arrhenius equation (**Figure 2**). It is noted that E_a is calculated when the glycerol conversion is less than 15 %. The E_a value for AuPd/ZnO-CuO (26.0 kJ·mol⁻¹) is lower than that for AuPd/ZnO (32.4 kJ·mol⁻¹) and

AuPd/CuO (40.0 kJ·mol⁻¹), confirming that the AuPd/ZnO-CuO catalyst could effectively lower the reaction energy barrier.

Table 1 Performance comparison table of different catalysts

Catalysts	TOF (h ⁻¹)	Selectivity (%) ^g					Max Yield(%)	C _{balance} (%)
		DHA	GCO	GLD	GLYA	others		
AuPd/CuO	26.7	-	-	-	-	-	9.84	100
AuPd/ZnO	100.0	-	-	-	-	-	36.4	99.1
Au/ZnO-CuO	194.3	76.1	10.2	1.2	0	12.5	54.2	98.2
Pd/ZnO-CuO	0	-	-	-	-	-	-	100
AuPd/ZnO-CuO ^a	644.8	76.1	6.6	0	0	17.3	56.6	98.8
AuPd/ZnO-CuO ^b	623.5	65.3	9.2	2.4	0	23.1	48.4	99.4
AuPd/ZnO-CuO ^c	687.1	86.0	6.4	0.3	0	7.3	65.5	97.5
Pt-Bi/MCM-41 ^d	260.4	62.6	-	10.6	26.6	0.2	52	-
Pt-Sb/CNTs ^e	-	70.0	-	10.0	18.0	2.0	52	-
Pt-Bi/Ac ^d	426.0	61.0	-	8.0	16.0	15.0	42	-
Pt/MgO/SBA-15 ^f	403.8	-	-	-	-	-	5.5	-

^aAu:Pd=10:1,Zn:Cu=10:1

^bAu:Pd=10:1,Zn:Cu=1:10

^cAu:Pd=10:1,Zn:Cu=1:1

^dReaction conditions: 5.0 g catalyst, 175 mL 1.0 M glycerol solution , 75 °C and P=2.1bar, 400 mL/min of O₂.

^eReaction conditions: 30 mL, 0.1 g/mL glycerol aqueous solution, glycerol/Pt molar ratio=890, 60 °C and 150 mL/min of O₂.

^fReaction conditions: 0.2 catalyst, 25 mL aqueous solution of glycerol (0.22 M), glycerol/Pt molar ration 530, 60 °C, 1 MPa O₂, 8 h.

^gSelectivity at glycerol conversion of 75 %.

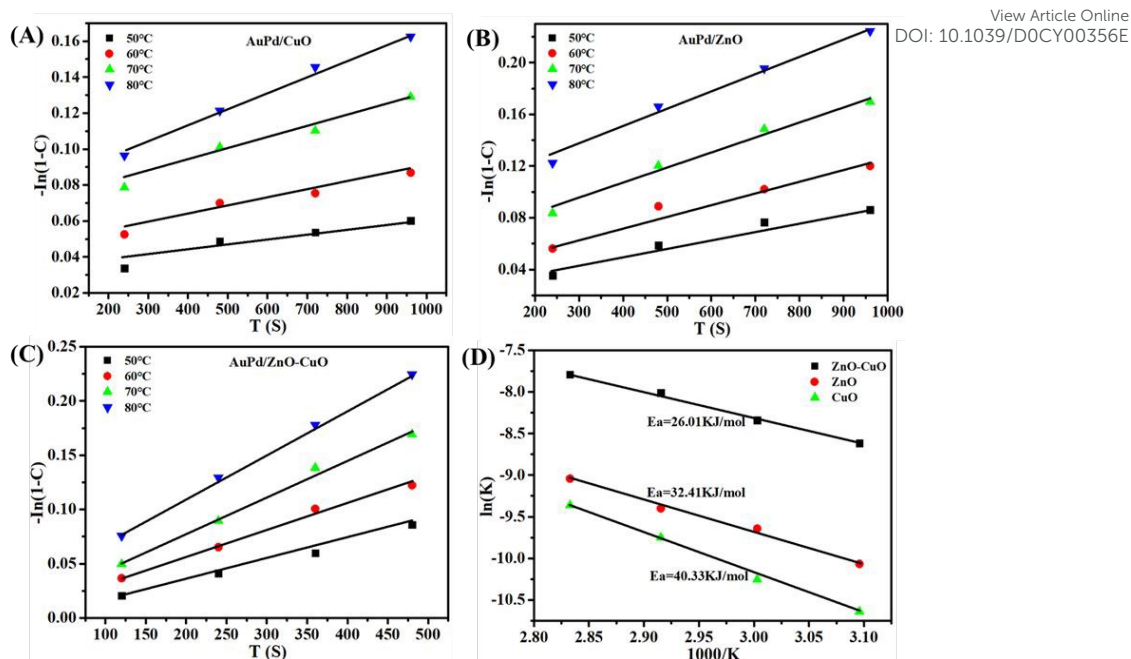


Figure 2. Time-conversion plots for AuPd/CuO catalyst (A), AuPd/ZnO catalyst (B), AuPd/ZnO-CuO catalyst (C), and Arrhenius plots for glycerol oxidation (D).

3.2 Geometric structure and vacancies in supports and catalysts

From the powder XRD pattern (**Figure 3(A)**), it is proved that our synthesized CuO is a monoclinic crystal structure [32]. The CuO phase has lattice parameters of $a=4.685$ Å, $b=3.426$ Å, $c=5.130$ Å (JCPDS No. 45-0937). XRD pattern of ZnO displays a wurtzite structural phase [33,34], and the lattice parameter is $a=3.250$ Å, $b=3.250$ Å, $c=5.207$ Å (JCPDS No.36-1451). The XRD pattern of ZnO-CuO shows space group symmetry of ZnO and CuO. Any hydroxide phases such as $\text{Zn}(\text{OH})_2$ and $\text{Cu}(\text{OH})_2$ or any other impurity phases are absent. **Figure 3(B)** is the local amplification at $30\text{-}40^\circ$ and shows that the characteristic peaks of ZnO and CuO in the ZnO-CuO sample shift, suggesting that the prepared support is not a simple physical mixture. In detail, the characteristic peaks representing CuO shifts to a low angle (0.063°), and ZnO shifts to a high angle (0.069°), indicating the lattice expansion and lattice shrinkage happens over CuO and ZnO respectively. According to the literature, the close radius of Zn^{2+} (0.74 Å) and Cu^{2+} (0.73 Å) ions results in the easy of Zn^{2+} and Cu^{2+} to enter the lattice of each other [35-37]. Moreover, the XRD pattern of the catalysts was also obtained. It could be seen that Au or Pd species are not detected in **Figure S1(A)**, indicating the

NPs are in a small and uniform state. In **Figure S1(B)**, the ZnO-CuO also shows peak shift compared with the pure sample. Therefore, it could be known that the ZnO-CuO could maintain its stable structure after the deposition of AuPd species.

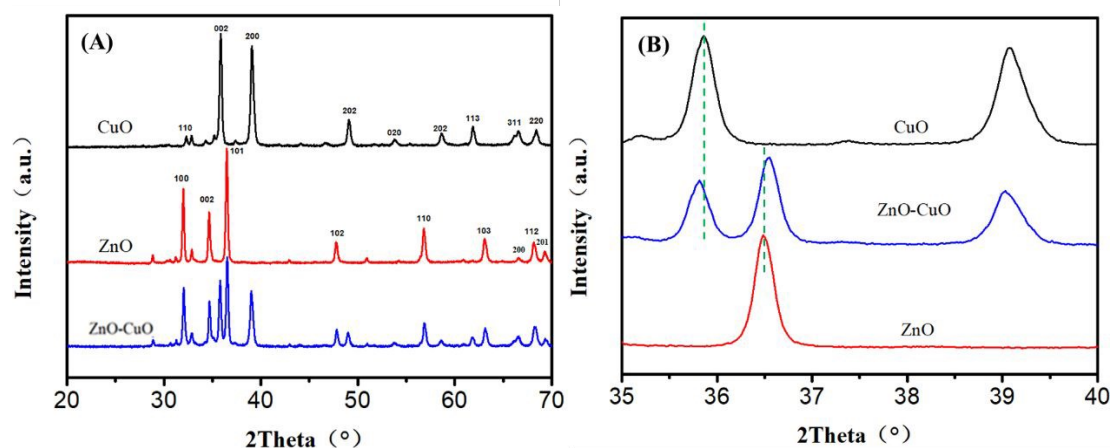


Figure 3. Powder XRD patterns of CuO, ZnO and ZnO-CuO supports **(A)**, partially enlarged views **(B)**.

It can be seen from **Figure 4(A)** that the support has a nanosheet structure, and the average size is less than 300 nm. In **Figure 4(C-F)**, Zn and Cu in the support are evenly distributed and there is no agglomeration. Further, we exam the Zn/Cu ratio on the surface and in the bulk phase. From STEM-EDS pictures, the atom ratio of Zn/Cu on the surface of ZnO-CuO is 0.90 [38]. The ICP results show that the molar ratio of Zn/Cu in the support is 0.93, which is close to the STEM-EDS result and the theoretical ratio [39]. Hence, it can be considered that the elements in the ZnO-CuO support are evenly distributed. The specific surface area and pore size of the three supports are obtained by BET analysis, and similar results are seen (**Table 2**).

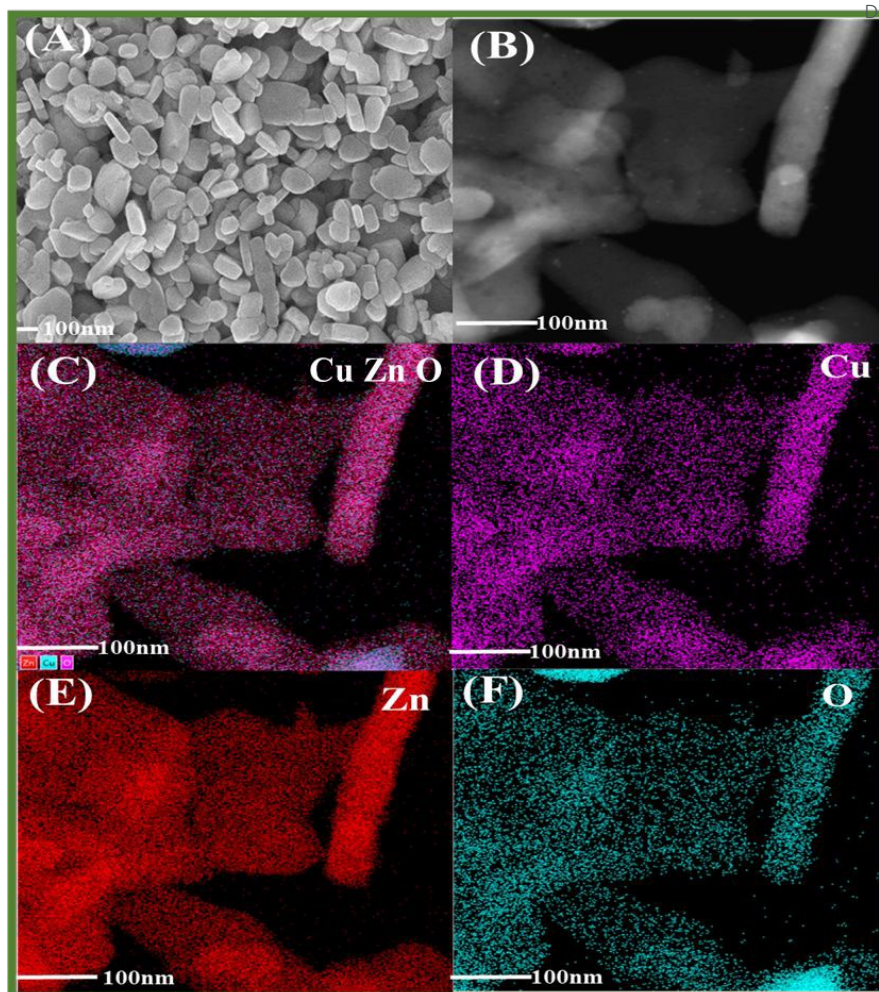


Figure 4. SEM (A) and STEM-EDS (B-F) mapping images of ZnO-CuO.

Table 2. Support specific surface, pore capacity and element distribution

Supports	Specific surface	Average pore	Zn/Cu	Zn/Cu
	area (m ² /g)	diameter (nm)	molar ratio ^a	molar ratio ^b
CuO	3.3	7.67	--	--
ZnO	4.0	8.60	--	--
ZnO-CuO	5.4	7.41	0.93:1	0.90:1

^a based on ICP result

^b based on EDS

It is known that the vibration wave number of M-O bond in metal compounds usually locates at 400-600 cm⁻¹ in FTIR. In **Figure 5**, the stretching vibration peak of Cu-O bond is seen at 528.5 cm⁻¹, and the wavenumber of Zn-O bond is at 439.7 cm⁻¹[40]. In the case of the ZnO-CuO sample, the stretching vibration of both ZnO and

CuO is observed. Moreover, the Cu-O bond in ZnO-CuO is red-shifted by 13 cm^{-1} , and the Zn-O bond is blue-shifted by 7 cm^{-1} . According to the XRD results, this shift is due to the doping of Zn ions into the CuO crystal lattice, which causes the expansion of CuO crystal lattice. On the contrary, the shrinkage of ZnO lattice leads to the blue-shift [41].

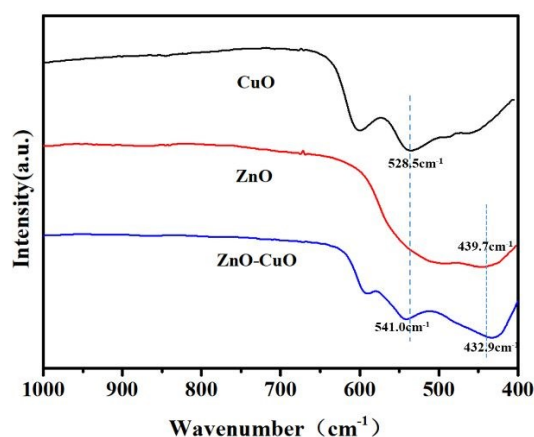


Figure 5. FTIR spectra of CuO, ZnO and ZnO-CuO supports.

In Raman spectroscopy, CuO has nine regional central optical phonon modes and only one A_g and two B_g modes have Raman activity. In **Figure 6(A)**, the peak of CuO at 274.9 cm^{-1} could be attributed to the A_g mode, and the peak of 322.2 cm^{-1} and 606.3 cm^{-1} corresponds to the B_g modes [42]. Irwin reported that the three Raman peaks in CuO only arise from the vibrations of the oxygen atoms [43]. ZnO shows characteristic peaks at 328.1 cm^{-1} and 434.7 cm^{-1} , which is corresponding to the $2E_2$ (low) and $2E_2$ (high) modes of ZnO. $2E_2$ (low) is due to the vibration of Zn atoms and $2E_2$ (high) is due to the oxygen sublattice vibration. The existence of these two modes reflects ZnO possesses a wurtzite structure with good crystallinity [44]. Moreover, the signal observed at 579.8 cm^{-1} could be attributed to the characteristic peak of oxygen vacancy in ZnO. For ZnO-CuO sample, the characteristic peaks reflecting the good crystallinity of ZnO disappear and similar and we observe red-shift spectra of CuO. It can be presumed that the presence of Cu-O destroys the regular Zn-O bond. The red shift could be ascribed to the reduction of grain size or the generation of defects. According to Scherrer formula, the crystal phase size in single CuO is 0.606 nm , while the CuO crystal phase size in ZnO-CuO increases to 0.727 nm . Therefore, we consider this red

shift is caused by the increase of defective sites [45]. After the deposition of AuPd species, the red shift could also be found in AuPd/ZnO-CuO catalyst. Noticeably, a new peak appears in AuPd/ZnO and AuPd/ZnO-CuO catalysts around 569 cm^{-1} (**Figure 6(B)**). This peak could be attributed to the oxygen vacancies near the AuPd NPs due to the insert of AuPd nanoparticles into the lattice of ZnO, indicating the doping of AuPd NPs has a positive effect on increasing the oxygen vacancies of the catalysts [46].

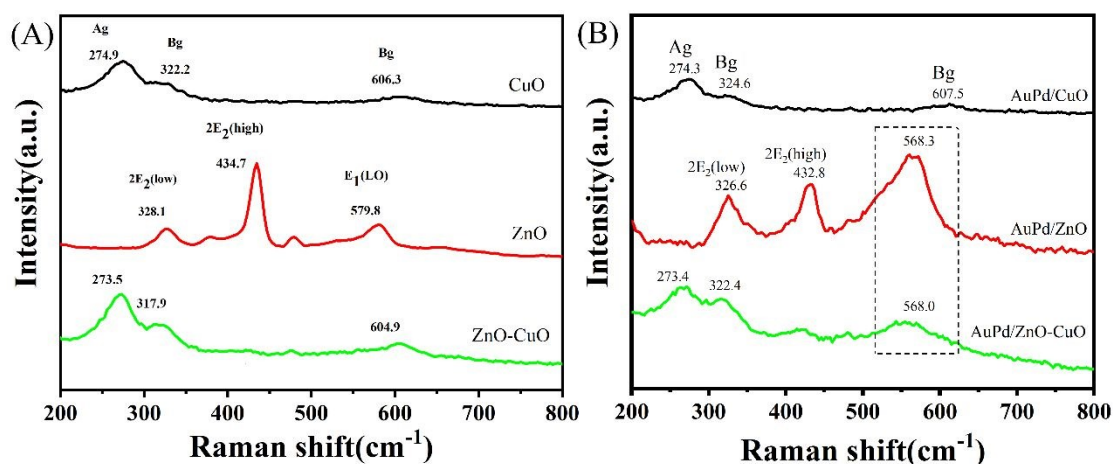


Figure 6. Raman spectra of CuO, ZnO and ZnO-CuO supports (A); AuPd/CuO, AuPd/ZnO and AuPd/ZnO-CuO supports.

The amount of oxygen defects on the surface of the support is detected by XPS analysis. As shown in **Figure 7**, there are three types of oxygen species attributed to lattice oxygen (L-O), oxygen vacancies (V-O), and chemically adsorbed oxygen (A-O) from the low binding energy (B.E) to high B.E [47]. We calculate the proportion of each oxygen species and find that the lattice oxygen content of ZnO-CuO is 15.6 %, which is lower than that of CuO (30.4 %) and ZnO (22.9 %). The content of oxygen defects on the surface of ZnO-CuO is 75.7 %, which is higher than that of CuO (62.5 %) and ZnO (62.1 %). Theoretically, the ratio of the metal ion to the lattice oxygen in the three supports is 1 and this ratio indicates the content of oxygen vacancies on the surface [48]. We then calculate the ratio of meta/lattice oxygen (**Table 3**) and find that the ratio in CuO, ZnO, and ZnO-CuO supports are 1.05, 1.38, and 2.04, respectively. The highest ratio in ZnO-CuO confirms that more oxygen defects are generated on the surface of ZnO-CuO. Furthermore, we investigate the oxygen species of AuPd/ZnO-CuO catalysts with different Zn/Cu ratio. The XPS results show (**Figure S2**) that the different

proportions Zn/Cu results in different oxygen vacancy content and AuPd/ZnO-CuO (Zn: Cu= 1: 1) catalyst has the highest content of oxygen vacancies (79.7 %). It could be inferred that due to the similar atomic radius 1: 1 of Zn/Cu is the most beneficial ratio for Zn and Cu to enter the lattice of each other to create oxygen vacancies. As a result, AuPd/ZnO-CuO (Zn: Cu= 1: 1) with high concentration of oxygen vacancies exhibits the preferred catalytic performance.

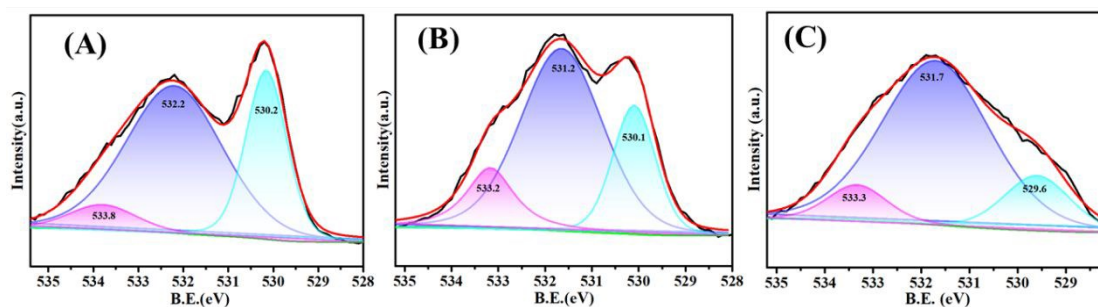


Figure 7. O_{1s} XPS spectra of CuO (A), ZnO (B), ZnO-CuO (C).

Table 3. Atomic Concentration Calculated from XPS.

Support	M(%)	O(%)	Oxygen			M/L-O	
			species(%)				
			L-O	V-O	A-O		
CuO	24.3	75.7	30.4	62.5	7.1	1.05	
ZnO	24.1	75.9	22.9	62.1	15.0	1.38	
ZnO-CuO	Cu 10.3	Zn 13.8	75.9	15.6	75.7	8.7	2.04

Electron paramagnetic resonance (EPR) is a sensitive technique for detecting unpaired electron oxygen vacancies. In **Figure 8(A)**, due to the characteristics of CuO itself, the signal related to its oxygen vacancy cannot be observed in EPR [49]. As for ZnO and ZnO-CuO, we can see that there are obvious characteristic peaks around $g=1.96$. According to the reported literature, the characteristic peak intensity could represent the level of oxygen vacancies [50]. It can be seen that the characteristic peak intensity of ZnO-CuO is significantly higher than that of ZnO, indicating more oxygen vacancies exist in the ZnO-CuO support. In quantitative analysis, the content of oxygen

vacancies per milligram of the sample is performed. The content of oxygen vacancies in the ZnO-CuO is $2.73 \times 10^{13} \text{ mg}^{-1}$, which is 2.5 times higher than that in ZnO. Together with XPS results, we consider that ZnO-CuO possesses the highest amount of oxygen defects in the three samples. We further collect the EPR spectrum of the catalysts (**Figure S3**). The results also indicate that AuPd/ZnO-CuO catalyst has the highest content of oxygen defects ($1.6 \times 10^{15} \text{ mg}^{-1}$). It should be mentioned that the concentration of oxygen defects in AuPd/ZnO and AuPd/ZnO-CuO catalysts increase compared with the pure ZnO and ZnO-CuO. This could be explained as the doping of AuPd has a positive effect of the increasing concentration of the supports, and a similar result has also been found in the Raman spectra.

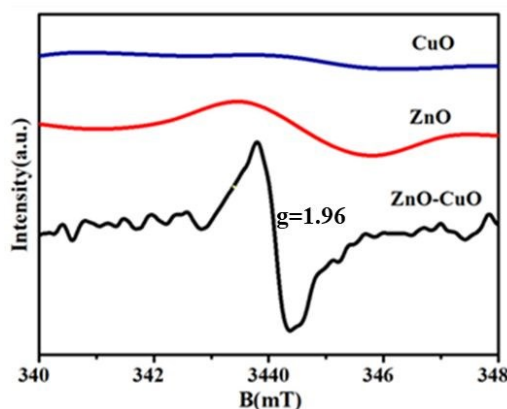


Figure 8. EPR spectra of the supports.

3.3. Investigation of AuPd species

Figure 9 shows the HRTEM images of AuPd/CuO, AuPd/ZnO, AuPd/ZnO-CuO catalysts. In **Figure 9(A-C)**, most of the AuPd NPs are elliptical and uniformly distributed on the support without agglomeration. We randomly select more than 400 particles starting from any of the three samples. **Figure 9(G-I)** has a particle size distribution range of 1 to 6 nm and the average particle size of AuPd/CuO, AuPd/ZnO, AuPd/ZnO-CuO is 4.3 nm, 4.1 nm, and 3.1 nm, respectively. It can be seen from **Figure 9(D-F)** that the lattice spacing of the active components in AuPd/CuO, AuPd/ZnO, AuPd/ZnO-CuO is 0.230 nm, 0.228 nm, 0.232 nm, and all are between that of Pd (111) and Au (111) [51]. HAADF-STEM could obtain more insights into the bimetallic metal

particle. The line scan results (**Figure 10**) indicate that the concentration of Pd increases with that of Au, confirming the alloy structure of Au-Pd particles [52]. It can be seen that AuPd/ZnO-CuO catalyst has the smallest particle size in all the bimetallic catalysts, which is one of the reasons for its improved catalytic performance.

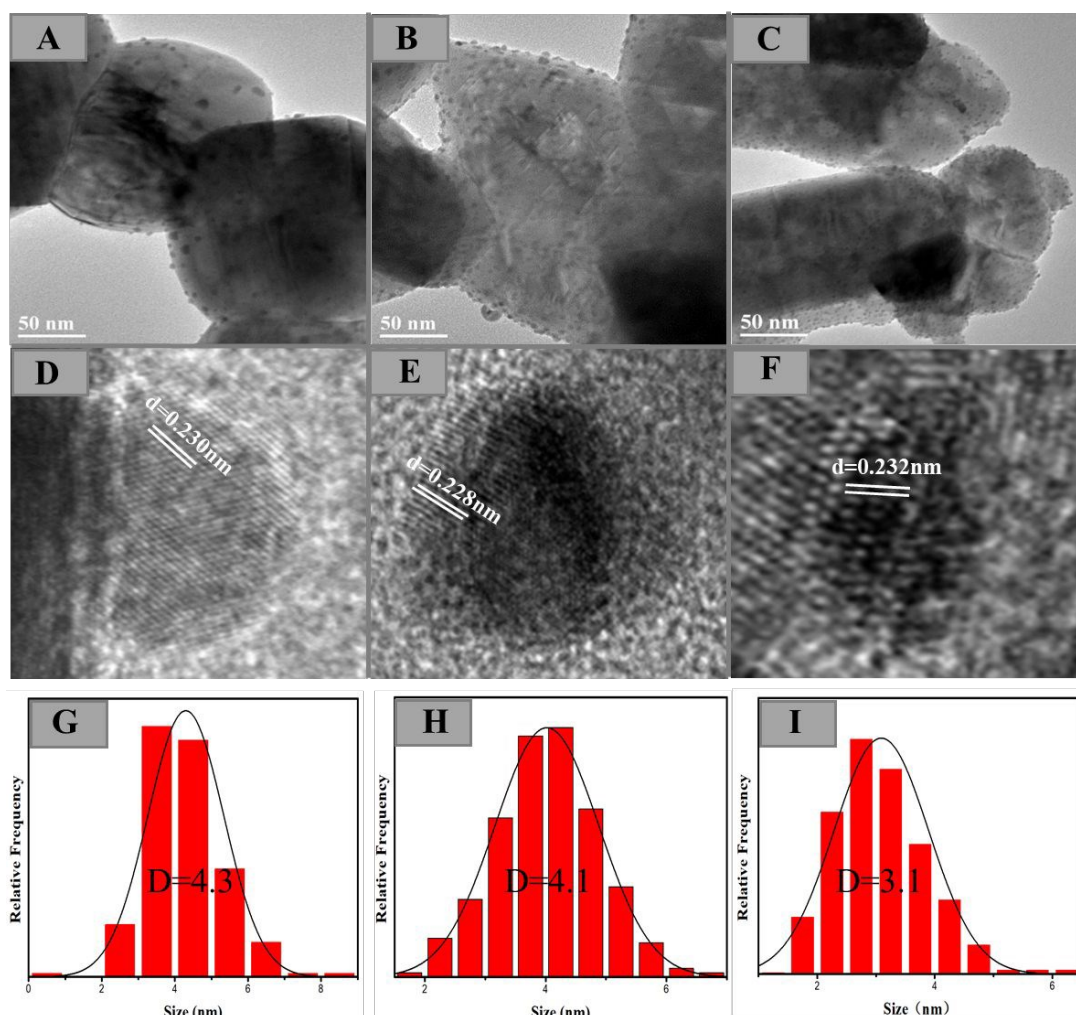


Figure 9. HRTEM images of AuPd/CuO (**A, D**), AuPd/ZnO (**B, E**), AuPd/ZnO-CuO (**C, F**), histograms of the particle size distribution of AuPd/CuO (**G**), AuPd/ZnO (**H**), AuPd/ZnO-CuO (**I**).

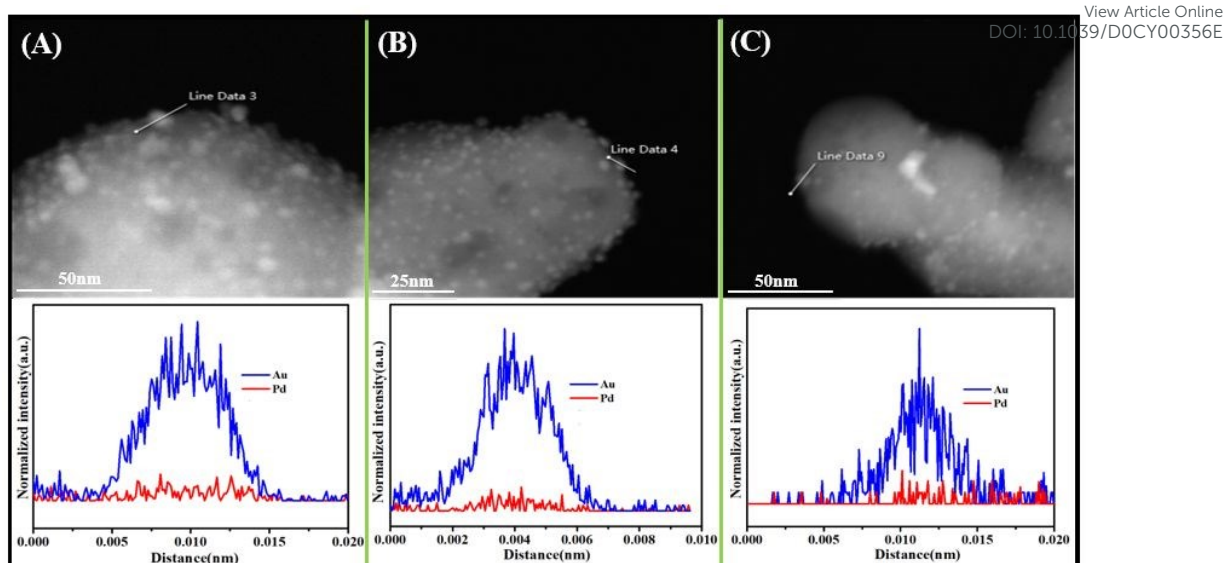
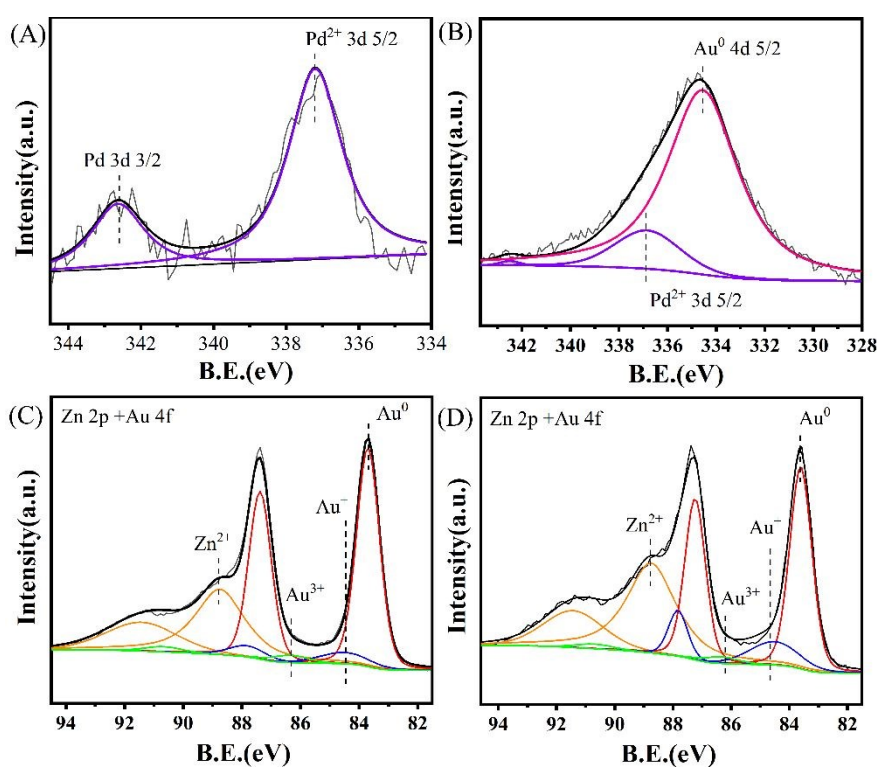


Figure 10. HAADF-STEM images and line scans of AuPd/CuO (A), AuPd/ZnO (B), AuPd/ZnO-CuO (C).

In **Table 1**, the AuPd/ZnO-CuO catalyst shows the best catalytic performance and Au/ZnO-CuO catalyst exhibits only 194.3 h^{-1} in TOF. Meanwhile, Pd/ZnO-CuO catalyst has no catalytic performance. Taking the preparation method into account, the catalysts were calcinated in the air to get the final catalysts and Pd in the catalysts may exist in an oxidized state. Therefore, we carried out the XPS analysis to investigate the Au and Pd species and the synergetic effect. As shown in **Figure 11(A)**, the Pd in Pd/ZnO-CuO catalyst shows only Pd^{2+} state. Due to the high Au/Pd ratio in the AuPd/ZnO-CuO catalyst, the 3d orbital of Pd is covered by the Au 4d orbital (**Figure 11(B)**). Through the deconvolution, we find that there is only Pd^{2+} in AuPd/ZnO-CuO catalyst, implying that Pd^{2+} serves as the catalyst additive. Moreover, we study the Au 4f orbital in Au/ZnO-CuO and Pd/ZnO-CuO catalysts to get the content of Au^0 and $\text{Au}^{+/3+}$ (**Figure 11(C) and (D)**). The results (**Table S1**) show that the AuPd/ZnO-CuO catalyst has 23.6 % of $\text{Au}^{+/3+}$ species and Au/ZnO-CuO catalyst only processes 14 % of $\text{Au}^{+/3+}$ species. For Au species, the positive Au will enhance the H elimination of the secondary hydroxyl group and then increase the activity of the catalysts [53]. Moreover, our previous research found that glycerol and DHA competed for adsorption on the catalyst [54]. Therefore, the increased $\text{Au}^{+/3+}$ species by the introduction of Pd element could inhibit the over oxidation of DHA and then improve the selectivity of the catalyst.



View Article Online
 DOI: 10.1039/D0CY00356E

Figure 11. XPS spectrum of Pd/ZnO-CuO catalyst (A), Au/ZnO-CuO catalyst (C), and AuPd/ZnO-CuO catalyst (B) and (D).

3.4. Reaction mechanism

We introduce the FTIR study of glycerol of the catalysts to investigate the effect of the oxygen vacancy Zn content of the reaction. As shown in **Figure 12**, the adsorption of glycerol on metal oxide could be defined as γ (related to the adsorption of the primary hydroxyl group of glycerol on the surface) and β (related to the adsorption of the secondary hydroxyl group of glycerol on the surface) [55]. In β region, it could be seen that AuPd/ZnO and AuPd/CuO catalysts show inconspicuous adsorption of the secondary hydroxyl group of glycerol. Notably, the AuPd/ZnO-CuO catalyst shows a β adsorption peak around 1152 cm^{-1} . According to our previous work [53], the increased concentration of oxygen vacancies of the catalysts is closely connected with the adsorption of the secondary hydroxyl group of glycerol. At the same time, the γ region of the three catalysts shows no significant difference in wavenumber, indicating that the adsorption of the primary hydroxyl group is not sensitive to the concentration of oxygen vacancies of the catalysts. It should be mentioned that the AuPd/CuO catalyst shows the lowest adsorption intensity of these catalysts, implying a weak adsorption

ability of glycerol in CuO, and this might be a reason for the low activity of the AuPd/CuO catalyst. Moreover, glyceraldehyde, the oxidation product of the primary hydroxyl group, is not detected in our reaction system. Therefore, we consider that the oxygen vacancies on the catalyst surface provided adsorption sites for the secondary hydroxyl of glycerol.

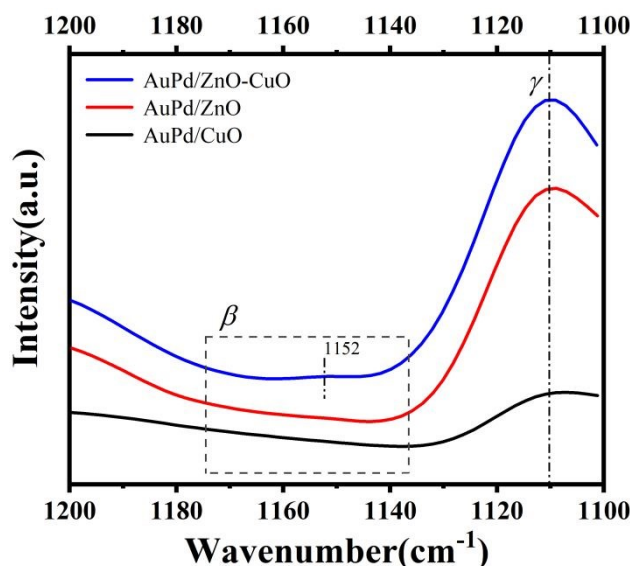


Figure 12. FTIR of glycerol of AuPd/ZnO-CuO, AuPd/ZnO and AuPd/CuO catalysts.

In AuPd/ZnO-CuO system, a reasonable reaction mechanism is further proposed. As shown in **Figure 13**, O₂ is dissociated on the AuPd NPs to form atomic oxygen (O*), which then combines with H₂O to generate peroxides (OOH*) and hydroxyl (OH*) species. Meanwhile, the secondary hydroxyl group of glycerol is adsorbed on the oxygen vacancies adjacent to metal ions. In the second step, the hydroxyl group (OH*) on AuPd combines with the H in the secondary hydroxyl group of glycerol to form H₂O. Then OOH* on AuPd cleaves the β-H of glycerol to produce DHA and H₂O₂, which is a kinetically rate-limiting step [56]. Eventually, DHA and H₂O₂ desorb from the active site and the reaction sites return to the original state. In this system, the small particle size could enhance the ability to dissociate oxygen. More importantly, the rich surface oxygen vacancies could effectively increase the activation of secondary hydroxyl groups of glycerol. Therefore, AuPd/ZnO-CuO with the smallest AuPd NPs and the most concentration of oxygen defects display the preferred catalytic performance.

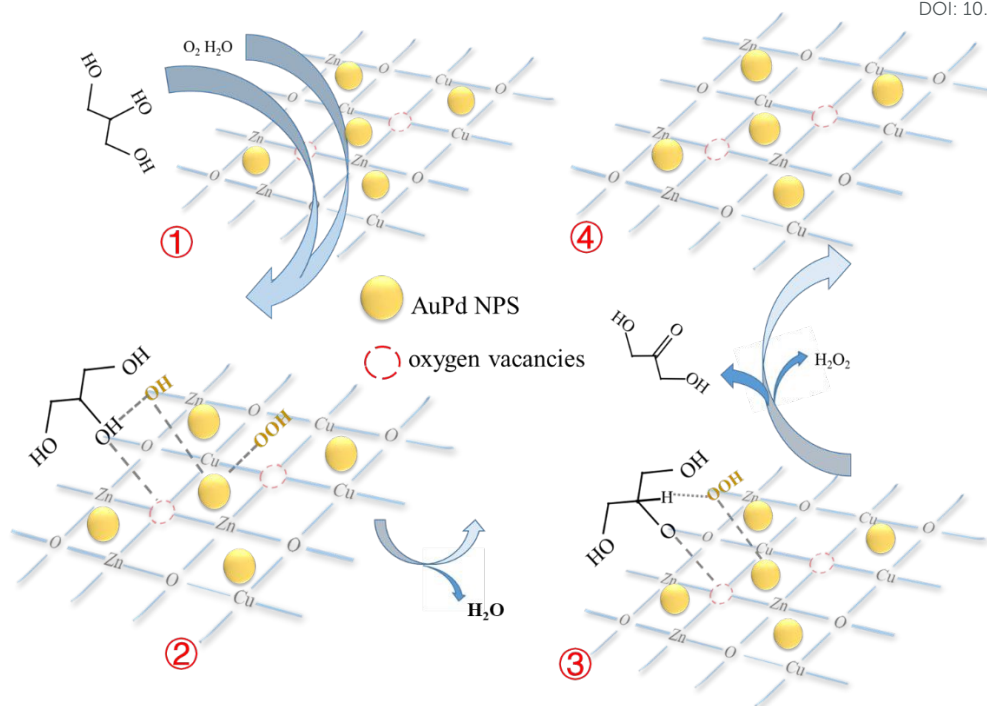


Figure 13. Oxidation of the secondary hydroxyl group in glycerol at the AuPd/ZnO-CuO interface

4. Conclusions

In this paper, a ZnO-CuO oxide is prepared by a simple precipitation method. This composite oxide is then used as support to prepare AuPd/ZnO-CuO catalysts, which applies in the selective oxidation of glycerol. The catalytic evaluation shows that the AuPd/ZnO-CuO catalyst possesses increased catalytic activity and selectivity. When the reaction time is 2 h, the conversion of the catalyst is 80% and the DHA yield can reach 65%. Moreover, The TOF value of AuPd/ZnO-CuO is as high as 687.1 h⁻¹, which is 3.5 times that of Au/ZnO-CuO and 6 times that of AuPd/ZnO. HRTEM result shows that AuPd/ZnO-CuO has the smallest active component particles among the three alloy catalysts, which is an important reason for its improved catalytic activity. Raman result displays that the Cu atoms destroy the ordered regular structure of Zn-O in ZnO, which leads to the improvement in the concentration of oxygen vacancies characterized by XPS and EPR analysis. Therefore, we consider the increase in surface oxygen vacancies in AuPd/ZnO-CuO provides more adsorption activation sites for the secondary hydroxyl oxidation of glycerol and effectively improves the catalytic performance.

Acknowledgments

This work was supported by the National Key R&D Program of China (No. 2017YFA0206804) and the National Natural Science Foundation of China (21706009, 21521005).

Conflicts of interest

There are no conflicts to declare.

Appendix A. Supplementary material

References

- [1] A. Villa, N. Dimitratos, C. E. Chan-Thaw, C. Hammond, L. Prati, G. J. Hutchings, *Acc. Chem. Res.*, 2015, 48, 1403-1412.
- [2] C. H. Zhou, J. N. Beltramini, Y. X. Fan, G. Q. Lu, *Chem. Soc. Rev.*, 2008, 37, 527-549.
- [3] G. Dodekatos, S. Schünemann, H. Tüysüz, *ACS Catal.*, 2018, 8, 6301-6333.
- [4] A. Behr, J. Eilting, K. Irawadi, J. Leschinski, F. Lindner, *Green Chem.*, 2008, 10, 13-30.
- [5] B. Katryniok, H. Kimura, E. Skrzyńska, J. Girardon, P. Fongarland, M. Capron, R. Ducoulombier, N. Mimura, S. Paul, F. Dumeignil, *Green Chem.*, 2011, 13, 1960-1979.
- [6] N. Gupta, O. Khavryuchenko, A. Villa, D. Su, *ChemSusChem.*, 10 (2017) 3030-3034.
- [7] G. M. Lari, C. Mondelli, J. Pérez-Ramírez, *ACS Catal.*, 5 (2015) 1453-1461.
- [8] X. Wang, G. Wu, F. Wang, K. Ding, F. Zhang, X. Liu, Y. Xue, *Catal. Commun.*, 28 (2012) 73-76.
- [9] S. A. Kondrat, P. J. Miedziak, M. Douthwaite, G. L. Brett, T. E. Davies, D. J. Morgan, J. K. Edwards, D. W. Knight, C. J. Kiely, S. H. Taylor, *ChemSusChem.*, 7 (2014) 1326-1334.
- [10] C. D. Evans, S. A. Kondrat, P. J. Smith, T. D. Manning, P. J. Miedziak, G. L. Brett, R. D. Armstrong, J. K. Bartley, S. H. Taylor, M. J. Rosseinsky, *Faraday Discuss.*, 188 (2016) 427-450.
- [11] Y. Shen, Y. Li, H. Liu, *J. Energy Chem.*, 24 (2015) 669-673.
- [12] X. Ning, Y. Li, H. Yu, F. Peng, H. Wang, Y. Yang, *J. Catal.*, 335 (2016) 95-104.
- [13] S. Hirasawa, H. Watanabe, T. Kizuka, Y. Nakagawa, K. Tomishige, *J. Catal.*, 300 (2013) 205-216.
- [14] S. Carrettin, P. McMorn, P. Johnston, K. Griffin, C. J. Kiely, G. J. Hutchings, *Phys. Chem. Chem. Phys.*, 5 (2003) 1329-1336.
- [15] S. Carrettin, P. McMorn, P. Johnston, K. Griffin, C. J. Kiely, G. A. Attard, G. J. Hutchings, *Top. Catal.*, 27 (2004) 131-136.
- [16] S. Carrettin, P. McMorn, P. Johnston, K. Griffin, G. J. Hutchings, *Chem. Commun.*, 696-697 (2002).
- [17] Z. Yuan, Z. Gao, B. Q. Xu, *J. Catal.*, 36 (2015) 1543-1551.
- [18] A. Villa, N. Dimitratos, C. E. Chan-Thaw, C. Hammond, L. Prati, G. J. Hutchings, *Acc. Chem. Res.*, 48 (2015) 1403-1412.
- [19] S. Schünemann, G. Dodekatos, H. Tüysüz, *Chem. Mater.*, 27 (2015) 7743-7750.
- [20] S. S. Liu, K. Q. Sun, B. Q. Xu, *ACS Catal.*, 4 (2014) 2226-2230.
- [21] G. D. Wu, G. Q. Zhao, J. H. Sun, X. Z. Cao, Y. F. He, J. T. Feng, D. Q. Li, *Journal of Catalysis.*, 377 (2019) 271-282.
- [22] Y. N. Pan, G. D. Wu, Y. F. He, J. T. Feng, D. Q. Li, *Journal of Catalysis.*, 369 (2019) 222-232.
- [23] N. Dimitratos, J. A. Lopez-Sanchez, D. Lennon, Porta, Prati, Villa, *Catal. Lett.*, 2006, 108, 147-153.
- [24] C. L. Xu, Y. Q. Du, C. Li, J. Yang, G. Yang, *Appl. Catal., B.*, 2015, 164, 334-343.
- [25] C. L. Xu, Y. Q. Du, C. Li, J. Yang, G. Yang, *Appl. Catal., B.*, 2015, 164, 334-343.
- [26] A. Villa, S. Campisi, K. M. H. Mohammed, N. Dimitratos, F. Vindigni, M. Manzoli, W. Jones, M. Bowker, G. J. Hutchings, L. Prati, *Catal. Sci. Technol.*, 2015, 5, 1126-1132.
- [27] Y. F. Wang, Z. Chen, P. Han, Y. H. Du, Z. X. Gu, X. Xu, G. F. Zheng, *ACS Catal.*, 2018, 8, 7113-7119.
- [28] M. Shekhar, J. Wang, W. S. Lee, W. D. Williams, S. M. Kim, E. A. Stach, J. T. Miller, W. N.

- Delgass, F. H. Ribeiro, *J. Am. Chem. Soc.*, 134 (2012) 4700-4708.
- [29] R. Van Hardeveld, F. Hartog, *Surf. Sci.*, 15 (1969) 189-230.
- [30] Y. Xiao, Z. J. Zhao, G. Jeffrey, G. M. Xiao, A. Varma, *AIChE. Journal.*, 63(2):705-715 July 2016.
- [31] X. Z. Duan, Y. F. Zhang, M. J. Pan, H. Dong, B. X. Chen, Y. Y. Ma, G. Q. X. G. Zhou, *AIChE. Journal.*, 2018, 64: 3979-3987.
- [32] Q. B. Zhang, K. L. Zhang, D. G. Xu, G. C. Yang, H. Hung, F. Nie, C. M. Liu, S. H. Yang, *Materials. Science.*, 60 (2014) 208-337.
- [33] L. Yang, Y. Tang, A. Hu, X. Chen, K. Liang, L. Zhang, *Physica. B.*, 403 (2008) 2230-2234.
- [34] V. Etacheri, R. Roshan, V. Kumar, *ACS. Appl. Mater. Interf.*, 4 (2012) 2717-2725.
- [35] S. Sonal, K. Japinder, N. Tsering, S. Rimi, *Physica. B.*, 407 (2012) 1223-1226.
- [36] E. Michal, L. Jonathan, G. Aharon, B. Ehud, *Adv. Funct. Mater.*, 2014, 24, 1382-1390.
- [37] C. L. Hsu, Y. D. Gao, Y. S. Chen, T. J. Hsueh, *ACS. Appl. Mater. Interfaces.*, 2014 6, 6, 4277-4285.
- [38] A. N. Pinheiro, S. B. Fe. D. Santos, M. J. D. S. Júnior, T. P. Braga, V. N. Freire, A. Valentini, *Catal. Sci. Technol.* 2018,8, 443-458.
- [39] Y. Kon, T. Fujitani, T. Nakashima, T. Murayama, W. Ueda, *Catal. Sci. Technol.*, 2018,8, 4618-4625.
- [40] S. Harisha, J. Archanab, M. Sabarinathana, M. Navaneethana, K.D. Nishab, S. Ponnusamyb, C. Muthamizhchelvanb, H. Ikedaa, D.K. Aswalc, Y. Hayakawa, *Applied. Surface. Science.*, 418 (2017) 103-112.
- [41] X. S. Ye., J. Sha, Z. K. Jiao, *Nano. Structrued. Materials.*, 1997, 8(7); 945-951.
- [42] J. F. Xu, W. Ji, Z. X. Shen, W. S. Li, S. H. Tang, X. R. Ye, D. Z. Jia and X. Q. Xin, *J. Raman. Spectrosc.*, 30, 413-415 (1999).
- [43] J. C. Irwin, T. Wei, J. Franck, *J. Phys. Condens. Matter.*, 3, 299 (1991).
- [44] A. K. Rana, Y. Kumar, P. Rajput, S. N. Jha, D. Bhattacharyya, P. M. Shirage, *ACS Appl. Mater. Interfaces.*, 2017, 9, 7691-7700.
- [45] J. F. Xu, W. Ji, Z. X. Shen, W. S. Li, S. H. Tang, X. R. Ye, D. Z. Jia, X. Q. Xin, *J. Raman Spectrosc.* 30, 413-415 (1999).
- [46] J. Wang, Y. Xia, Y. Dong, R. Chen, L. Xiang, S. Komarneni, *Appl. Catal. B Environ.* 192 (2016) 8-16.
- [47] W. Annan, P. Qing, Y. D. Li, *Chem. Mater.*, 2011, 23, 3217-3222.
- [48] C. M. Olmos, L. E. Chinchilla, A. Villa, J. J. Delgado, A. B. Hungría, G. Blanco, L. Prati, J. J. Calvino, X. W. Chen, *Journal of Catalysis.*, 375 (2019) 44-55.
- [49] G. Tofghi, X. J. Yu, H. Lichtenberg, D. E. Doronkin, W. Wang, C. Wöll, Y. M. Wang, J. D. Grunwaldt, *ACS. Catal.*, 2019, 9, 5462-5473.
- [50] H. Q. Tan, Z. Zhao, W. B. Zhu, E. N. Coker, B. Li, M. Zheng, W. X. Yu, H. Y. Fan, Z. C. Sun, *ACS. Appl. Mater. Interfaces.*, 2014, 6, 19184-19190.
- [51] Y. L. He, Z. S. Fishman, K. R. Yang, B. Ortiz, C. L. Liu, J. Goldsamt, V. S. Batista, L. D. Pfefferle, *J. Am. Chem. Soc.*, 2018, 140, 1824-1833.
- [52] A. Dehelean, A. Popa, S. Rada, E. Cule, *J. Magn. Magn. Mater.* 381(2015)131-137.
- [53] G. D. Wu, G. Q. Zhao, J. H. Sun, X. Z. Cao, Y. F. He, J. T. Feng, D. Q. Li, *J. Catal.*, 377 (2019) 271-282.

[54] Pan, Y., Wu, G., He, Y., Feng, J., & Li, D, J.Catal. 369 (2019): 222-232.

View Article Online
DOI: 10.1039/D0CY00356E

[55] Copeland, J. R., Santillan, I. A., Schimming, S. M., Ewbank, J. L., & Sievers, C, J. Phys. Chem. C 2013, 117, 21413–21425.

[56].B. N. Zope, D. D. Hibbitts, M. Neurock, R. J. Davis, Science., 330 (2010) 74.

